Precision Engineering 49 (2017) 146–159

Contents lists available at ScienceDirect

Precision Engineering

journal homepage: www.elsevier.com/locate/precision

Principle of elastic averaging for rapid precision design

Tat Joo Teo [a,b,*], Alexander H. Slocum [a]

[a] Precision Engineering Research Group, Department of Mechanical Engineering, Massachusetts Institute of Technology, Cambridge, MA 02139, United States
[b] Mechatronics Group, Singapore Institute of Manufacturing Technology, Agency for Science, Technology and Research, Singapore 138634, Singapore

ARTICLE INFO

Article history:
Received 8 December 2016
Received in revised form 11 January 2017
Accepted 3 February 2017
Available online 16 February 2017

Keywords:
Elastic averaging
Over-constrained design
Flexure
Precision alignment and repeatability

ABSTRACT

Elastic averaging has worked well throughout history to help create precision machines. With the advent of rapid fabrication processes such as additive manufacturing, abrasive waterjet machining, and laser cutting etc., parts fabricated from these processes can be designed with special elastic features that "average out" the uncertainty in dimension tolerances and manufacturing errors as a collective system at very low cost. This paper presents the principle of elastic averaging and explores simple flexure design to create elastic averaging features within parts for precision alignment and assembly applications. A first-order analytical model and a quick estimation approach is introduced to predict the alignment errors and the repeatability of these parts. Experimental results show that a part with four elastic averaging features was capable of achieving precision assembly with another mating part even after huge errors were purposefully introduced to the mating features. Results also show that the part can achieve sub-micron level repeatability after more than 20 trials of removals and assemblies. Lastly, analytical simulations show that repeatability of the part can be further improved by increasing the number of elastic contacts. All these results suggest that the assemblies of rapid fabricated parts with elastic averaging features can be as precise as those made from conventional machine centers.

1. Introduction

Rapid fabrication processes such as waterjet, laser cutting, and Additive Manufacturing (AM) etc., are perceived as good technology for producing prototypes rather than producing functional parts for precision applications. In the case of AM technology, it has been widely recognized that 3D printed alloy-based parts have rough surfaces and the poor tolerance that are limited by the size of the powder, and the spot size of the lasers. Hence, these parts require secondary removal processes (or post-processing) to enhance the surface finish and improve the tolerance. With state-of-the-art AM technology, it is unlikely that 3D printed parts (without post-processing) can be used in precision applications where sub-micron repeatability and accuracy are required. Similarly, neither abrasive waterjet machining nor laser cutting process can reproduce the high dimension tolerances delivered by conventional milling, turning, and grinding fabrication processes.

The principle of elastic averaging has been known and practiced for eons [1–7] but is often overlooked in the modern world of Computer-Aided Design (CAD) where everything appears exact with perceived perfection. Yet even for precise-machined metal parts, all too often dowel pins are relied upon but the high stiffness of pins pressed into holes requires clearance, and as a result accuracy is compromised. In the case of fitting precision machine elements, e.g., ball bearings etc., into/onto not so precise features of a part, tolerance rings, which are commercially available [8], are often used to provide local radial compliance. Similarly, axial wave springs also accomplish this function. On the other hand, the ubiquitous LEGO™ brick mates have exquisite precision [9] even to bricks made decades ago. Indeed, the same principle has even been applied to MEMs devices [6], wafer [10] and micro-fluidic devices [11] but has yet been applied to rapid fabricated parts, making them applicable for precision applications without post-processing.

This paper presents the use of elastic averaging to design rapid fabricated parts that can be used in precision alignment and assembly applications. By using the underlying physics of elastic bodies motion and force interactions, these parts can be designed with elastic features that can "average out" the uncertainty in dimension tolerances and manufacturing errors as a collective system. The paper is organized with the following sections that present the principle of elastic averaging, a general modeling approach to obtain first-order analytical model to predict the misalignment errors and the repeatability of parts with elastic averaging features, the experimental investigations that were conducted to evaluate

* Corresponding author at: A*STAR, 2 Fusionopolis Way, #08-04, Innovis, Singapore 138634, Singapore.
E-mail address: tjteo@SIMTech.a-star.edu.sg (T.J. Teo).

https://doi.org/10.1016/j.precisioneng.2017.02.003
0141-6359/

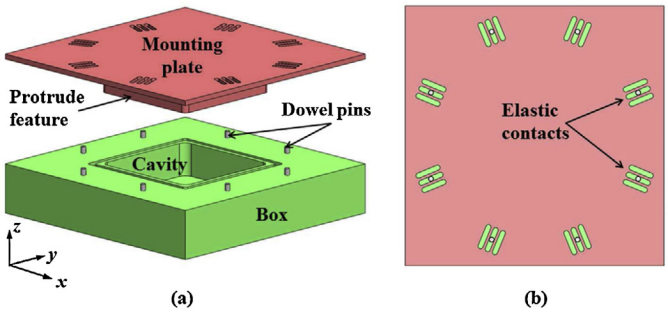

Fig. 1. (a) Illustration of a box with a cavity that has a mounting plate to seal the top portion. (b) Top view of the mounting top that has eight symmetrical elastic contacts to locate the seal the box with eight guiding dowel pins.

the analytical predictions and effectiveness of elastic averaging, and the simulation results on how repeatability can be improved with respect to the number of elastic features.

2. Principle of elastic averaging

Unlike a kinematic coupling that interfaces two rigid-body parts based on exact constraint design [12], elastic averaging requires one of the interfacing parts to have over-constrained rigid features while the other interfacing part made of a network of compliance members equal to the number of those over-constrained rigid features. Think of one of the classic epitomes of elastic averaging: the use of multiple blade flexures to support a high precision optical element. Indeed, any structure can be thought of as a collection of springs of stiffness and the connection between structures is no different. Fig. 1a shows a box with a cavity in the middle that has a mounting plate to seal the top portion. The protruded feature of the mounting plate, which matches the cavity of the box, forms a slight clearance gap between the walls of the feature and the cavity. In order to maintain the gap within the desired tolerances, the mounting plate needs to be precisely located in the middle of the box. Instead of using a traditional arrangement of two or three dowel pins mating with slightly oversized holes (or a hole and a slot) to locate the mounting plate, the principle of elastic averaging can be used to precisely locate the protruded feature relative to the cavity and constrain the top mounting plate to the box.

The mounting plate will require three Degrees-Of-Freedom (DOF) in-plane constraints, i.e., along the x- and y-axis, and about the z-axis. For the traditional approach of having three dowel pins in slightly oversized holes or pushing against the edges of three slots, it is an almost exact constraint design since one dowel pin constrains the motion along the x-axis while the remaining two constrain the motion along the y-axis, and about the z-axis, except when parasitic forces move the dowel pins away from the slot edges. However, having an eight dowel pins layout as illustrated in Fig. 1b will be an over constraint design and requires the mounting plate to have similar number of elastic contacts to average out the errors. When both parts are brought together, the effective elastic contacts between them will be forced into equilibrium, hence some forces may be very high, causing local yielding. In addition, a geometric equilibrium will be achieved, which may or may not result in the desired position between both parts. As a result, the key is to deterministically design these elastic contacts such that when forced together with the dowel pins, none of them will be over stressed, and the resulting relative position between the two parts is within desired tolerance. Thus, a desirable and deterministic global stiffness of the assembly must be achieved.

To design such an assembly, the first thing to decide is whether the role of the elastic averaging function, i.e., is it there to align the parts which are then clamped together so global stiffness comes from the clamped (e.g., bolted) joint or is it there to align the parts and provide the global desired stiffness once both parts are aligned. The former would be for a structural assembly and the latter would be the case for a printed gear to be mounted on a shaft. This can be accomplished with the following thought process:

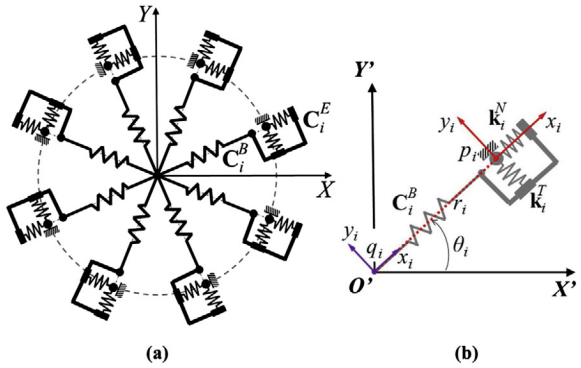

Fig. 2. Schematic of (a) a generic mounting plate with systematical and evenly distributed elastic contacts, and (b) the orientation of the each elastic contact w.r.t. frame O'.

- Define the desired accuracy of the assembly (δ_A).
- Define the expected geometric mismatch of the parts (manufacturing error) (δ_m). This is also the overall amount that elastic contacts can be expected to have to deform to accommodate manufacturing errors.
- The factor N_s to achieve better performance is in a ratio; $N_s = \delta_m/\delta_A$.
- Assuming the manufacturing errors will be randomly distributed, the number of elastic contacts, N, required to "average out" the errors will be $N = N_s{}^2$ conservatively.
- Define the desired stiffness of the assembled joint, k_a.
- Set the number of elastic contacts.

The final step is to formulate an analytical model that predicts the relative 3-DOF in-plane deviations between the two parts when brought together.

3. General modeling approach

The general modeling approach is to first obtain the stiffness model of the mounting plate with respect to (w.r.t.) the center of the box (or base). Next, determine the total force vector and moment applied at the center of the mounting plate due to the potential manufacturing errors such as the position offset from the individual dowel pin, variations in the flexure thickness etc. Subsequently, the deviations along the x- and y-axis, and about the z-axis can be obtained using the Hooke's Law

$$\begin{bmatrix} \Delta X \\ \Delta Y \\ \Theta Z \end{bmatrix} = [\mathbf{K}_{SYS}]^{-1} \begin{bmatrix} F_X \\ F_Y \\ M_Z \end{bmatrix} \tag{1}$$

3.1. Stiffness modeling of the entire system

The mounting plate can be represented by a series of springs connected in parallel with the dowel pins being the ground of the entire system as illustrated in Fig. 2a. A global coordinate frame, $O\{X, Y\}$, is attached to the center of the base and a local coordinate frame, $O'\{x, y\}$ is attached to the center of the mounting plate to describe the relative motion of frame O' w.r.t. frame O. Hence, frame O and frame O' overlap each other at initial condition. Each elastic

contact has a local coordinate frame, $p\{x, y\}$, that is attached to the center of the dowel pin as shown in Fig. 2b. As each dowel pin is mounted to the base, the orientation and the distance of each frame p w.r.t. frame O are represented by θ_i and r_i respectively.

As shown in Fig. 2b, the stiffness of each elastic contact, $\mathbf{K}_i^E$, will be the sum of the tangential spring stiffness, $\mathbf{k}_i^T$, and normal spring stiffness, $\mathbf{k}_i^N$, where i denotes the numbering of each elastic contact. (Note: $\mathbf{k}_i^N$ must be oriented to the same orientation as $\mathbf{k}_i^T$ before summation.) For planar motion, the orientation matrix, $\mathbf{G}$, is given as

$$\mathbf{G}_i = \begin{bmatrix} \cos\theta_i & \cos(\theta_i + 90^\circ) & 0 \\ \sin\theta_i & \sin(\theta_i + 90^\circ) & 0 \\ 0 & 0 & 1 \end{bmatrix} \tag{2}$$

The distance of frame p w.r.t. frame O' is governed by the Jacobian matrix, $\mathbf{J}_i$, expressed as

$$\mathbf{J}_i = \begin{bmatrix} 1 & 0 & -r_{y,i} \\ 0 & 1 & r_{x,i} \\ 0 & 0 & 1 \end{bmatrix} \tag{3}$$

All elastic contacts are connected in parallel by the main body of the mounting plate. Hence, each elastic contact is connected in series to a portion of the main body to form a segment of the overall stiffness as illustrated in Fig. 2a. It is important to account for the compliance of the main body because it has finite stiffness and different geometries will affect the overall system stiffness. With a local coordinate frame, $q\{x, y\}$, being attached to the center of the mounting plate, the compliance of each segment is the sum of the compliance of a portion of the main body, $\mathbf{C}_i^B$, and the compliance of each elastic, $\mathbf{C}_i^E$. With all the segments connected in parallel, the overall stiffness of the mounting plate is the sum of all segments' stiffness.

3.2. Coupling effect between the elastic contacts

For each elastic contact, there is a force–displacement coupling effect with its neighboring elastic contacts. This coupling effect has been commonly used in vibration and numerical models [13–15]. For elastic averaging, this coupling effect has certain degrees of impact on the stiffness of individual elastic contact. According to the Maxwell's reciprocal theorem, when a linear continuum elastic body is subjected to two different sets of forces, the work done from the two sets of forces and the respective resultant displacements is equal [16]. Refer to Fig. 3a, Case I shows that a force, F_1, acting at Point-1 will result in a displacement at Point-1, δ_1, and at Point-2, δ_2. In Case II, if the applied force, F_2, at Point-2 is equal to F_1 of Case I then δ_1 will equal δ_2 of Case I [17]. Hence, the Maxwell's reciprocal theorem governs the symmetry of the stiffness or compliance matrix of a linear continuum elastic system.

The coupling effect in Cases I and II can be represented using the two tangential springs from the elastic contacts within the first quadrant of the spring system illustrated in Fig. 2a. To simplify the example, both springs are rotated to the same orientation and their fixed points are aligned horizontally as shown in Fig. 3a. The relationship between the displacements and the forces can be expressed as

$$\begin{bmatrix} F_1 \\ F_2 \end{bmatrix} = \begin{bmatrix} K_{11} & K_{12} \\ K_{21} & K_{22} \end{bmatrix} \begin{bmatrix} \delta_1 \\ \delta_2 \end{bmatrix} \tag{4}$$

Being a linear continuum elastic system, the stiffness matrix is symmetrical and the non-diagonal components are equal, i.e., $K_{12} = K_{21}$. As a result, K_{21} will affect the force or displacement at

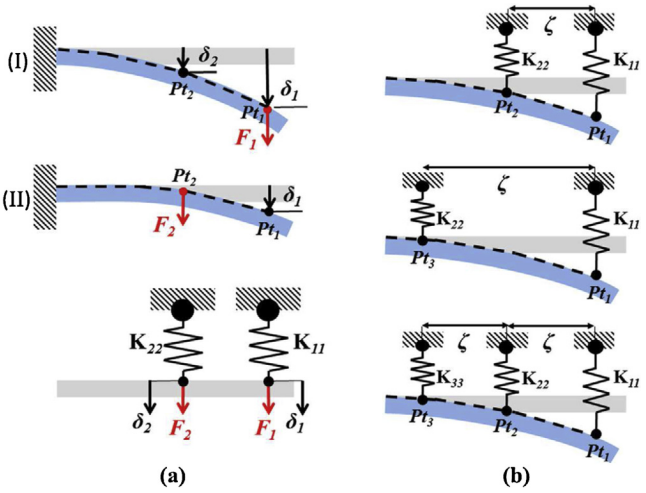

Fig. 3. Illustration of (a) a two springs system to represent coupling effect of two points on a deflected cantilever beam and (b) the effects of distance between the springs on the coupling effect.

Point-1. Similarly, K_{12} will also affect the force or displacement at Point-2. This shows that the non-diagonal components have direction contribution to the force–displacement coupling between both springs. By assuming that the non-diagonal component is equal to a certain percentage, λ, of the diagonal component, e.g., $K_{21} = \lambda K_{22}$, the stiffness matrix is re-written as

$$\begin{bmatrix} F_1 \\ F_2 \end{bmatrix} = \begin{bmatrix} K_{11} & \lambda K_{22} \\ \lambda K_{11} & K_{22} \end{bmatrix} \begin{bmatrix} \delta_1 \\ \delta_2 \end{bmatrix} \tag{5}$$

where certain percentage of the stiffness from the neighboring elastic contacts is used to account for the coupling effect.

In addition, the distance between each individual elastic contact and its neighboring elastic contacts also contribute to the coupling effect. Refer to Fig. 3b, the displacement at Point-2 is represented by the 2nd spring placed at a distance, ζ, away from the 1st spring. If the 2nd spring is placed at Point-3, the distance increases, the force applied at Point-1 has less effect on the displacement at Point-3, and thus the coupling effect decreases. Once a 3rd spring is placed at Point-3, all three springs will be equally spaced. It is clear that the coupling effect has less influence beyond the nearest neighboring elastic contacts. By observing the Saint Venant's Principle, which states that any effect is essentially negligible after 3–5 characteristic dimensions [18], the coupling effect will be limited to a group of three elastic contacts whereby the effect will be negligible after 3ζ. Hence, only the nearest neighboring elastic contacts beside the individual elastic contact will contribute to the coupling effect. Using Fig. 3b as an example, the stiffness of K_{22} becomes

$$\mathbf{K}_{22} = \mathbf{K}_{22} + \lambda \cos\phi(\mathbf{K}_{11} + \mathbf{K}_{33}) \tag{6}$$

where ϕ represents the angle between these elastic contacts. In general, the coupling effect is not present for spacing $\geq 90^\circ$ for a circular configuration. Based on a symmetrical design concept, the elastic contacts are equally spaced. Hence, the angle between each contact is given as $\phi = 360^\circ/n$.

3.3. Equilibrium conditions and constraints

After obtaining the stiffness model of the entire system, the next step is to determine the total force vector and moment applied to the center of the mounting plate. There are two sets of forces that need to be determined for any elastic averaging problem. The first set of forces is a collection of forces generated by the deflections within the elastic contacts due to the location offset of the

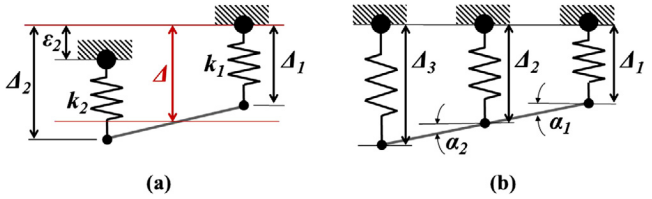

Fig. 4. Illustration of (a) a double-spring system with one spring having a position offset and (b) a group of three springs constrained by a rigid-link.

dowel pins and variations in the thickness of the flexure beams from manufacturing errors etc. The forces also include the resultant deflections caused by the equilibrium constraints. The second set of forces is a collection of reaction forces generated by the equilibrium conditions of the multi-springs system. Hence, it is important to understand how these equilibrium conditions and constraints are formed.

Using a double-spring system illustrated in Fig. 4a as an example whereby both springs are constrained by a rigid body with the dowel pins being the fixed ground, an offset, ε_2, generates a new equilibrium position. This new equilibrium position, Δ, due to the constraint of the rigid body and the equilibrium of forces is expressed as

$$\Delta = \frac{k_1\Delta_1 + k_2\Delta_2}{k_1 + k_2} \tag{7}$$

By assuming that $k_1 = k_2 = k$, Eq. (7) suggests that $\Delta = (\Delta_1 + \Delta_2)/2$. Hence, the equilibrium position will be the average of all the spring positions. For springs arranged in a circular configuration, the equilibrium position will be sum of all these offsets averaged by the number of springs.

Similarly for a group of three elastic contacts as illustrated in Fig. 4b, the relationship between the displacement of the three springs will be $\Delta_2 = 1/2(\Delta_1 + \Delta_3)$ based on the constraint condition of $\alpha_1 = \alpha_2$ and assuming the stiffness of the springs are equal. For a group of three elastic contacts arranged in a circular configuration, this relationship also suggest that the constraint ratio between the middle spring and its surrounding two springs is 1:0.5. This constraint ratio will be used to form the constraint matrix to determine the equilibrium displacement, δ, of each spring that is expressed as follows

$$\begin{bmatrix} \delta_2 \\ \delta_3 \\ \delta_1 \end{bmatrix} = \begin{bmatrix} 1 & 0.5 & 0.5 \\ 0.5 & 1 & 0.5 \\ 0.5 & 0.5 & 1 \end{bmatrix} \begin{bmatrix} \Delta_2 \\ \Delta_3 \\ \Delta_1 \end{bmatrix} \tag{8}$$

4. Case study: mounting plate with four elastic contacts

A mounting plate with four elastic contacts is used as a case study to demonstrate the effectiveness of the elastic averaging and how a first-order analytical model can be established based on the general modeling approach. Fig. 5a shows that each elastic contact is formed by a pair of flexures and a dowel pin, which is fixed to a base and press-fit into the slot in between. A global coordinate frame, $O\{X, Y\}$, is attached to the center of fixed base and a local coordinate frame, $O'\{x, y\}$ is attached to the center of the mounting plate. The dowel pins are equally spaced around the center of the base defined by a radius, r, w.r.t. the frame O. Similarly, all elastic contacts are equally spaced around the center of the mounting plate defined by r with elastic contact #1 (*EC-1*) positioned at 45° from the x-axis of frame O'.

Fig. 5b shows the schematic of the mounting plate represented as a four-spring system. Here, the compliance of each elastic contact is only represented by a tangential spring. By splitting into four segments, each segment consists of the compliance of a portion

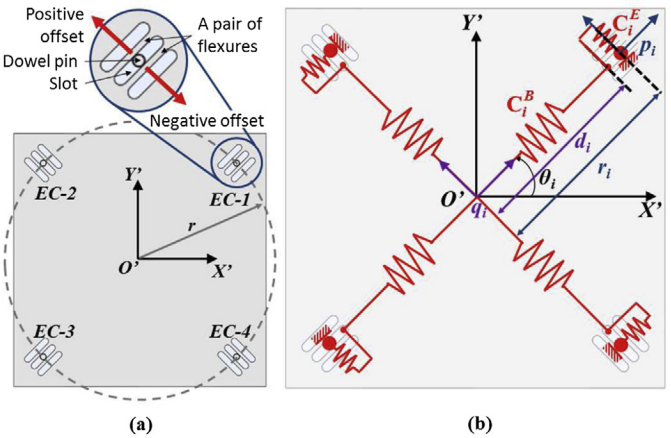

Fig. 5. Illustration of (a) a mounting plate with four elastic contacts and (b) its schematic representation as a four-spring system.

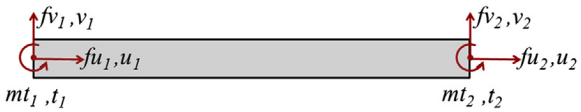

Fig. 6. Illustration of a beam element.

of the main body, $\mathbf{C}_i^B$, and the compliance of one elastic contact, $\mathbf{C}_i^E$, with i denoting the numbering of springs. Each elastic contact has a local coordinate frame, $p\{x, y\}$, attached to the center of each dowel pin. For each segment of the main body, a local coordinate frame, $q\{x, y\}$, is attached to the center of the mounting plate oriented in 45°.

In this case study, the dowel pins were purposefully offset (normal to the flexures) from its ideal location to determine the deviation along the x- and y-axis, and about the z-axis w.r.t. frame O. Using Hooke's Law expressed in Eq. (1) to predict such relative planar motion between frame O' and frame O, the first step is to determine the stiffness matrix of the mounting plate based on the schematic representation shown in Fig. 5b.

4.1. Stiffness model

A classical beam element is used to determine the stiffness matrix of each flexure within an elastic contact as shown in Fig. 6. The stiffness matrix of a beam element in 3-DOF planar motion is given as

$$\begin{bmatrix} fu_1 \\ fv_1 \\ mt_1 \\ fu_2 \\ fv_2 \\ mt_2 \end{bmatrix} = \begin{bmatrix} \frac{EA}{L} & 0 & 0 & -\frac{EA}{L} & 0 & 0 \\ 0 & \frac{12EI}{L^3} & \frac{6EI}{L^2} & 0 & -\frac{12EI}{L^3} & \frac{6EI}{L^2} \\ 0 & \frac{6EI}{L^2} & \frac{4EI}{L} & 0 & -\frac{6EI}{L^2} & \frac{2EI}{L} \\ -\frac{EA}{L} & 0 & 0 & \frac{EA}{L} & 0 & 0 \\ 0 & -\frac{12EI}{L^3} & -\frac{6EI}{L^2} & 0 & \frac{12EI}{L^3} & -\frac{6EI}{L^2} \\ 0 & \frac{6EI}{L^2} & \frac{2EI}{L} & 0 & -\frac{6EI}{L^2} & \frac{4EI}{L} \end{bmatrix} \begin{bmatrix} u_1 \\ v_1 \\ t_1 \\ u_2 \\ v_2 \\ t_2 \end{bmatrix} \tag{9}$$

where E is the Young's Modulus of the material, I is the moment of area, A represents the cross-sectional area and L represents the length of the beam element. The sign conventions of the force, f, and moment, m, and respective displacement of each axis are shown in Fig. 6.

In an ideal case, the dowel pin sits in the middle of a pair of flexures. Hence, it can be represented using four separate beam

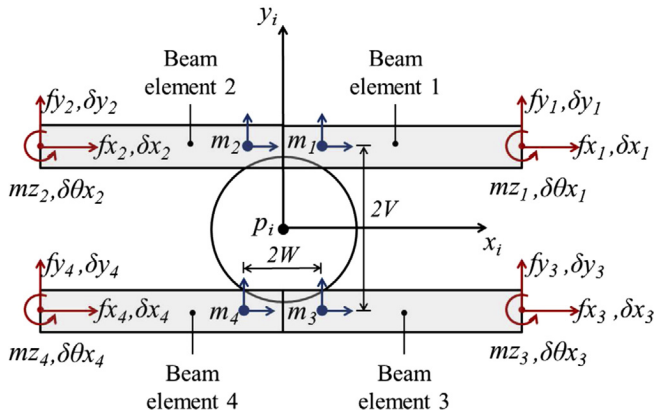

Fig. 7. Representing each elastic contact with four separate beam elements and their respective frames w.r.t. the center of the dowel pin.

elements where the fixed dowel pin becomes a constraint for each beam as illustrated in Fig. 7. Each beam element has a local coordinate frame, $m\{x, y\}$, attached on each beam element above the dowel pin. Hence, the location of frame m w.r.t. frame p is determined by half the distance between the center of the two beam elements, $2V$, and half the distance of the contact surface between the dowel pin and the pair of flexures, $2W$. Contact surface between the dowel pin and the pair of flexures exits because the slot between the pair of flexures needs to be smaller than the diameter of the dowel pin to generate forces that can constrain each pair of flexure at the desired position (see Section 4.2 for more detailed analysis.)

For each elastic contact, each flexure is treated as a beam fixed at both ends where the deflection occurs at the middle due to the offset of the dowel pin along the y-axis. Based on Eq. (9) and by considering L being half the total length of each flexure, i.e., $L = l/2$, the stiffness matrix of Beam element 1, $\mathbf{k}_{b1}$, and Beam element 2, $\mathbf{k}_{b2}$, are written as

$$\mathbf{k}_{b1} = \begin{bmatrix} \frac{EA}{2L} & 0 & 0 \\ 0 & \frac{12EI}{L^3} & -\frac{6EI}{L^2} \\ 0 & -\frac{6EI}{L^2} & \frac{4EI}{L} \end{bmatrix} \tag{10}$$

$$\mathbf{k}_{b2} = \begin{bmatrix} \frac{EA}{2L} & 0 & 0 \\ 0 & \frac{12EI}{L^3} & \frac{6EI}{L^2} \\ 0 & \frac{6EI}{L^2} & \frac{4EI}{L} \end{bmatrix} \tag{11}$$

By referring to Fig. 7, both beam elements are working in parallel along the y-axis. Hence, the stiffness matrix of each flexure is the sum of $\mathbf{k}_{b1}$ and $\mathbf{k}_{b2}$. As a result, the second diagonal component, k_{22}, of the stiffness matrix of each flexure beam will be $\frac{24EI}{L^3}$. With $L = l/2$, k_{22} from $\mathbf{k}_{b1} + \mathbf{k}_{b2}$ will be

$$k_{22} = \frac{192EI}{l^3} \tag{12}$$

Note that the first diagonal component of the matrices in Eqs. (10) and (11) is $\frac{EI}{2L}$ because both beam elements are in series along the x-axis. Refer to Fig. 7, the stiffness matrix of Beam element 3 is similar to Beam element 1, i.e., $\mathbf{k}_{b3} = \mathbf{k}_{b1}$ and the stiffness matrix of Beam element 4 is similar to Beam element 2, i.e., $\mathbf{k}_{b4} = \mathbf{k}_{b2}$. Subsequently, the stiffness matrix of each tangential spring w.r.t. the frame p, $\mathbf{k}_i^T$, is expressed as

$$\mathbf{k}_i^T = \sum_{j=1}^{4} \mathbf{J}_j^{-T} \mathbf{k}_{bj} \mathbf{J}_j^{-1} \tag{13}$$

where j denotes Beam elements 1–4. $\mathbf{J}_j$ is expressed in Eq. (3) and by referring to Fig. 7; $r_{y,1} = r_{y,2} = V$ and $r_{y,3} = r_{y,4} = -V$ while $r_{x,1} = r_{x,3} = W$ and $r_{x,2} = r_{x,4} = -W$. Next, the stiffness matrix of each tangential spring w.r.t. frame O', $\mathbf{K}_i^T$, is given as

$$\mathbf{K}_i^T = \mathbf{G}_i \mathbf{J}_i^{-T} \mathbf{k}_i^T \mathbf{J}_i^{-1} \mathbf{G}_i^T \tag{14}$$

where $\mathbf{G}_i$ is expressed in Eq. (2), $\mathbf{J}_i$ is expressed in Eq. (3) and refer to Fig. 5; $r_{y,i} = 0$ and $r_{x,i} = r_i$.

As mentioned in Section 3.2, there is a coupling effect from the neighboring elastic contacts and it affects the stiffness of individual elastic contact. Therefore, the stiffness matrix of each elastic contact is expressed as

$$\mathbf{K}_i^E = \mathbf{K}_i^T + \lambda \cos\phi (\mathbf{K}_{i+1}^T + \mathbf{K}_{i-1}^T) \tag{15}$$

where ϕ represents the space between each elastic contact and $\phi = 360^\circ/4 = 90^\circ$ in this case. Thus, the coupling effect from the nearest neighboring elastic contacts will not affect the in-between elastic contacts.

Next, the stiffness matrix of each segment w.r.t. frame O' is expressed as

$$\mathbf{K}_i^B = \mathbf{G}_i \mathbf{k}_i^B \mathbf{G}_i^T \tag{16}$$

where $\mathbf{G}_i$ is expressed in Eq. (2) and $\mathbf{k}_i^B$ is approximated using

$$\mathbf{k}_i^B = \begin{bmatrix} \frac{EA}{L} & 0 & 0 \\ 0 & \frac{12EI}{L^3} & -\frac{6EI}{L^2} \\ 0 & -\frac{6EI}{L^2} & \frac{4EI}{L} \end{bmatrix} \tag{17}$$

where $L = d$ and the remaining parameters are estimated based on a portion of the main body (see Appendix A). Finally, the stiffness matrix of the entire system is expressed as

$$\mathbf{K}_{SYS} = \sum_{i=1}^{4} \left(\mathbf{C}_i^B + \mathbf{C}_i^E\right)^{-1} \tag{18}$$

where $\mathbf{C}_i^B = (\mathbf{K}_i^B)^{-1}$ and $\mathbf{C}_i^E = (\mathbf{K}_i^E)^{-1}$.

4.2. Force and moment vectors

As shown in Fig. 5, the dowel pins are used to constrain the mounting plate to the base w.r.t. the frame O. Hence, each elastic contact must generate a pair of constraining forces that act on the dowel pin and these forces are generated by deflecting the flexures. The general approach is to press fit the dowel pin into the slot between a pair of flexures as shown in Fig. 8a. Hence, either the diameter of the dowel pin must be bigger than the slot or vice-versa. Depending on the tolerances to fit the dowel pin into the slot, the slot is typically smaller by 10–50 μm. This means that each flexure will deflect by half the amount of the difference between the dowel pin diameter and the slot. The forces generated by the pair of flexures are expressed as

$$\begin{aligned} F_{ai} &= k_{22}[(g_d + \varepsilon_i) - g_o] \\ F_{bi} &= k_{22}[(g_d - \varepsilon_i) - g_o] \end{aligned} \tag{19}$$

where g_o represents the original slot gap, g_d represents the slot gap after deflection, which is determined by the radius of the dowel pin,

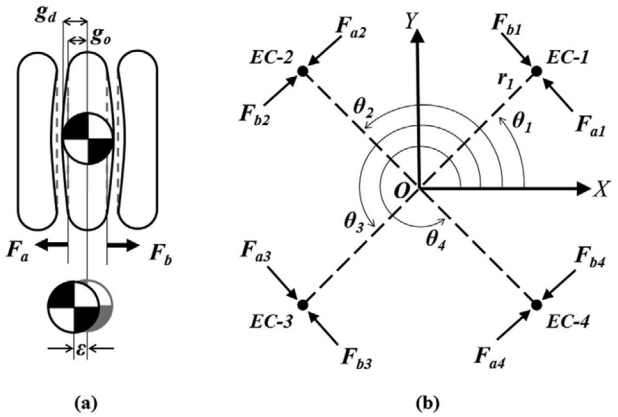

Fig. 8. Illustration of (a) a dowel pin within the slot from by a pair of flexures and (b) the respective force generated within each elastic contact.

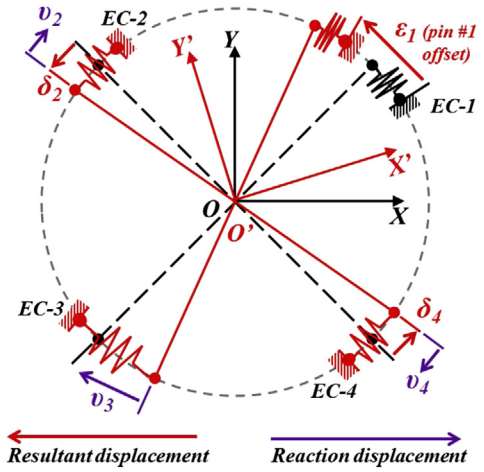

Fig. 9. Illustration of a dowel pin offset in EC-1 that causes a chain of resultant and reaction displacements within a four-spring system.

and ε represents the potential displacement due to the offsets of the dowel pins. Assuming that both flexures have same geometry and parameters, k_{22} is given in Eq. (12). Eq. (19) suggests that having a slot gap smaller than the diameter of dowel pin or vice-versa will generate a pair of forces that act on the dowel pin. The stress experienced by each flexure is given as $\sigma = 3E\delta h/L^2$ where $L = l/2$ [19] and must be within the yield strength of the material used to construct these flexures.

The pair of forces expressed in Eq. (19) are present in each elastic contact as illustrated in Fig. 8b. By resolving these pair of forces w.r.t. the frame O, Fig. 8b also shows the orientation of each pair of forces that are projected onto frame O. Assuming that the dowel pins are in their ideal positions and there is no offset from these dowel pins, the pair of forces will cancel out and there is no planar motion deviation from the mounting plate. Yet if there are offsets from these dowel pins, Eq. (19) is also used to determine the additional internal forces from each pair of flexures introduced into the system.

Based on Eq. (1), a vector comprising of forces and moment (force/moment) is required to determine the planar motion deviation of the mounting plate. As mentioned in Section 3.3, the final force/moment vector is the sum of two separate force/moment vectors w.r.t. the frame O, given as

$$\begin{bmatrix} F_X \\ F_Y \\ M_Z \end{bmatrix} = \begin{bmatrix} Fx_1 \\ Fy_1 \\ Mz_1 \end{bmatrix} + \begin{bmatrix} Fx_2 \\ Fy_2 \\ Mz_2 \end{bmatrix} \tag{20}$$

Using Eq. (19), these force/moment vectors are determined via two sets of displacements, i.e., the resultant and reaction displacements. Fig. 9 illustrates an example by offsetting the dowel pin within the EC-1 to cause a chain of resultant and reaction displacements within a four-spring system. First, the dowel pin offset, ε_1, will cause resultant displacements in EC-2, δ_2, and EC-4, δ_4, respectively due to the constraint condition as mentioned in Section 3.3. This set of resultant displacements is used to determine $[Fx_1\ Fy_1\ Mz_1]^{\mathrm{T}}$. Next, another set of force/moment vector occur instantaneously to drive each elastic contact to its equilibrium position. This set of forces can be determined by the reaction displacements, which occur as pairs and under the same constraint condition. With EC-1 and EC-3 working as a pair, ε_1 in the counter-clockwise direction causes a reaction displacement in EC-3, υ_3, in the opposing direction instantaneously. Due to the constraint condition, υ_3 then causes reaction displacements, i.e., υ_2 and υ_4, in both EC-2 and EC-4 respectively. Subsequently, this set of reaction displacements is used to determine $[Fx_2\ Fy_2\ Mz_2]^{\mathrm{T}}$.

4.2.1. Forces generated from the resultant displacements

Under the constraint condition, the resultant displacement, δ_i, in each elastic contact due to the offset of each dowel pin, ε_i, is expressed as

$$\hat{\mathrm{D}} = \mathbf{CM} \cdot \hat{\mathrm{O}}$$
$$\begin{bmatrix} \delta_1 \\ \delta_2 \\ \delta_3 \\ \delta_4 \end{bmatrix} = \begin{bmatrix} 1 & 0.5 & 0 & 0.5 \\ 0.5 & 1 & 0.5 & 0 \\ 0 & 0.5 & 1 & 0.5 \\ 0.5 & 0 & 0.5 & 1 \end{bmatrix} \begin{bmatrix} \varepsilon_1 \\ \varepsilon_2 \\ \varepsilon_3 \\ \varepsilon_4 \end{bmatrix} \tag{21}$$

where **CM** is the constraint matrix. Using Eq. (19) with $\varepsilon_i = \delta_i$ to determine each pair of forces (F_{ai} & F_{bi}) from each elastic contact, the first set of force/moment vector ($\rho = 1$) w.r.t. the global frame O as shown in Fig. 8b is obtained using

$$\begin{bmatrix} Fx_\rho \\ Fy_\rho \\ Mz_\rho \end{bmatrix} = \begin{bmatrix} \sum_{i=1}^{4} (F_{bi} - F_{ai}) \sin\theta_i \\ \sum_{i=1}^{4} (F_{ai} - F_{bi}) \cos\theta_i \\ \sum_{i=1}^{4} (F_{ai} - F_{bi}) \cdot r_i \end{bmatrix} \tag{22}$$

4.2.2. Forces generated from the reaction displacements

To determine reaction displacements, it is necessary to first predict the equilibrium position of individual elastic contacts due to the offsets of the dowel pins and the equilibrium positions, $\hat{\mathrm{E}}$, are approximated by

$$\hat{\mathrm{E}} = \mathbf{CM}' \cdot \hat{\mathrm{O}} \tag{23}$$

where $\mathbf{CM}' = \mathbf{CM}/n$ with n representing the number of elastic contacts (or springs). Subsequently, a set of reaction displacements, $\hat{\mathrm{R}}$, is given as

$$\hat{\mathrm{R}} = [\mathbf{Q} - \mathbf{CM}] \cdot (\hat{\mathrm{A}} - \hat{\mathrm{E}}) \tag{24}$$

where $\mathbf{Q}$ represents an unit matrix ($n \times n$) of all ones and $\hat{\mathrm{A}} = \hat{\mathbf{a}} \times (\epsilon/n)$ with $\hat{\mathbf{a}}$ representing an unit vector ($n \times 1$) of all ones and $\epsilon = \sum_i^n \varepsilon_i$. In this case study, Eq. (24) will return $\hat{\mathrm{R}} = [\upsilon_1\ \ \upsilon_2\ \ \upsilon_3\ \ \upsilon_4]$. Next, use Eq. (19) with $\varepsilon_i = \upsilon_i$ to determine each pair of forces (F_{ai} & F_{bi}) from each elastic contact and subsequently determine the second set of force/moment vector ($\rho = 2$) using Eq. (22). Lastly, the

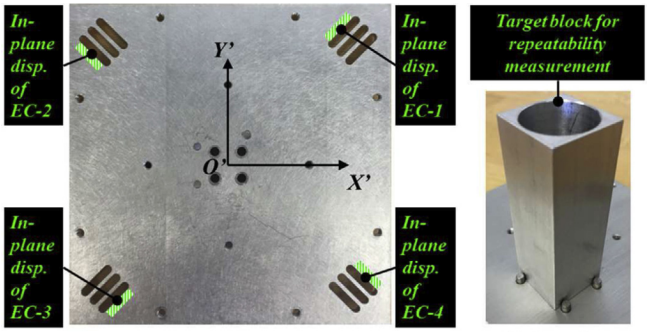

Fig. 10. Fabricated mounting plate with a target block mounted underneath it.

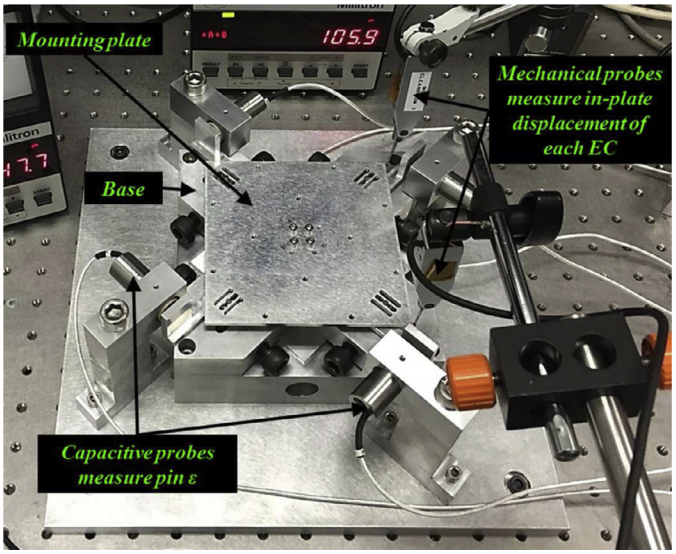

Fig. 11. Experimental setup with various measurement probes.

planar motion deviations w.r.t. frame *O* due to the offset of the dowel pins are determined using Eqs. (1), (18) and (20).

4.3. Experimental investigations

A prototype of the mounting plate was fabricated as shown in Fig. 10. It was fabricated by the milling method to obtain high dimensional tolerances since it was used to evaluate the accuracy of the analytical model and the effectiveness of those elastic averaging features. It is made of a square aluminium plate with a uniform thickness of 3 mm and the length, and thickness of each flexure is 12 mm and 1.5 mm respectively (note: all parameters are given in Appendix A). Each elastic contact has a designated location (highlighted in green as shown in Fig. 10) to measure its in-plane displacement. These in-plane displacements are the actual equilibrium positions of respective elastic contact due to the offset of dowel pins. In this investigation, these in-plane displacements are used to compute the actual deviations along the *x*- and *y*-axis, and about the *z*-axis w.r.t. the center of the fixed base.

The entire experimental setup is shown in Fig. 11 whereby the mounting plate was mounted onto the base (with pre-defined gaps in between them) using four dowel pins with tolerance fit between the pins and the flexures. In this setup, mechanical probe (MAHR; model: Millitron 1240) with a resolution of 0.1 μm were used to measure the in-plane displacements from each designated location on the mounting plate while capacitive probes (LION PRECISION; model: CPL290) with a resolution of 0.1 μm were used to measure

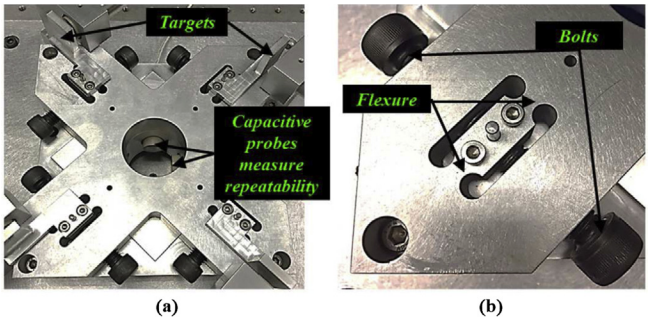

Fig. 12. (a) Base for the mounting plate with (b) flexure-based mechanism for displacing individual dowel pin.

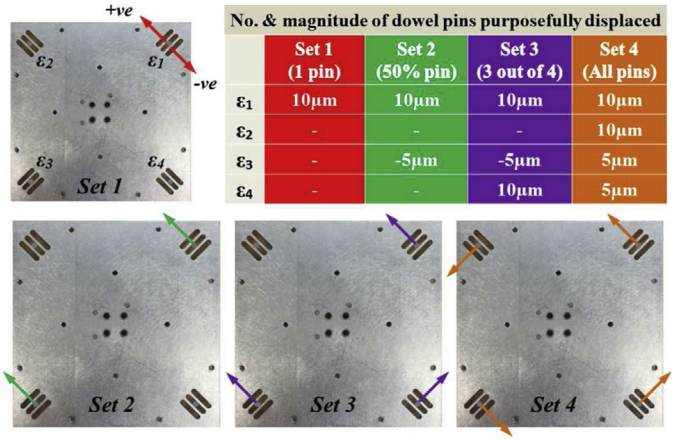

No. & magnitude of dowel pins purposefully displaced				
	Set 1 (1 pin)	Set 2 (50% pin)	Set 3 (3 out of 4)	Set 4 (All pins)
ε1	10μm	10μm	10μm	10μm
ε2	-	-	-	10μm
ε3	-	-5μm	-5μm	5μm
ε4	-	-	10μm	5μm

Fig. 13. Number and magnitude of dowel pins purposefully displaced to create deviations in the center during the experimental investigations.

the offsets from the dowel pins. The base was mounted on a larger piece of mounting plate that was bolted on an anti-vibration table. The base of the mounting plate was made with flexure-based mechanism to displace individual dowel pins as shown in Fig. 12. Each mechanism has a moving portion supported by a pair of flexures at the fixed ends. The dowel pin is located and fixed in the middle of the moving portion. M8 bolts were used to displace the dowel pin via the flexure-based mechanism and individual target block is mounted on each mechanism for the capacitive probe to measure the actual offset of each dowel pin.

Experimental investigations were conducted to evaluate the presented theoretical model that was used to predict the deviation of the mounting plate w.r.t. the center of the base due to the offset of the dowel pins. Most importantly, these investigations were also used to evaluate the effectiveness of the elastic averaging in averaging out the given errors. The investigations were conducted in four stages and each stage had a set of targeted dowel pin offsets as shown in Fig. 13. The first set only had the dowel pin in EC-1 being purposefully displaced to a targeted offset location and the second set was to displace 50% of the available dowel pins to their targeted offset locations. Third set was to displace all except one dowel pin and the fourth set was to displace all the dowel pins. Using the flexure-based mechanisms (Fig. 12b), the magnitude and direction of the targeted offsets are shown in Fig. 13 using different colors and arrows to illustrate the magnitude and directions for each set. The positive offset direction is in the counter-clockwise while the negative is in the clockwise direction.

During each investigation, the capacitive probes measured the offsets of the dowel pins and the mechanical probes measured the equilibrium positions from the designated locations on the mounting plate. Ten trials were conducted in each investigation. After

Table 1
Experimental and analytical results of the deviations of the prototype w.r.t. the center of the base due to different sets of targeted dowel pins offsets. Experimental results are averaged values of ten trials.

		Exp. results	Analytical results
Set 1	Deviation along the x-axis, ΔX (μm)	−0.88	−0.97
	Deviation along the y-axis, ΔY (μm)	0.85	0.97
	Deviation about the z-axis, ΘZ (μrad)	21.70	21.00
	Equilibrium position of EC-1 (μm)	2.62	2.50
	Equilibrium position of EC-2 (μm)	0.76	1.25
	Equilibrium position of EC-3 (μm)	0.20	0.00
	Equilibrium position of EC-4 (μm)	0.70	1.25
	Sum of equilibrium positions (μm)	4.28	5.00
Set 2	Deviation along the x-axis, ΔX (μm)	−1.51	−1.45
	Deviation along the y-axis, ΔY (μm)	1.39	1.45
	Deviation about the z-axis, ΘZ (μrad)	8.23	10.50
	Equilibrium position of EC-1 (μm)	2.58	2.50
	Equilibrium position of EC-2 (μm)	0.04	0.63
	Equilibrium position of EC-3 (μm)	−1.51	−1.26
	Equilibrium position of EC-4 (μm)	−0.15	0.63
	Sum of equilibrium positions (μm)	0.96	2.50
Set 3	Deviation along the x-axis, ΔX (μm)	−0.56	−0.48
	Deviation along the y-axis, ΔY (μm)	2.68	2.42
	Deviation about the z-axis, ΘZ (μrad)	35.50	31.40
	Equilibrium position of EC-1 (μm)	4.61	3.75
	Equilibrium position of EC-2 (μm)	0.30	0.63
	Equilibrium position of EC-3 (μm)	0.00	0.00
	Equilibrium position of EC-4 (μm)	3.18	3.13
	Sum of equilibrium positions (μm)	8.09	7.50
Set 4	Deviation along the x-axis, ΔX (μm)	−1.23	−0.97
	Deviation along the y-axis, ΔY (μm)	0.24	0.00
	Deviation about the z-axis, ΘZ (μrad)	66.10	62.90
	Equilibrium position of EC-1 (μm)	5.34	4.38
	Equilibrium position of EC-2 (μm)	5.21	4.38
	Equilibrium position of EC-3 (μm)	3.25	3.13
	Equilibrium position of EC-4 (μm)	3.80	3.13
	Sum of equilibrium positions (μm)	17.60	15.00

each trial, the measured equilibrium positions were used to determine the actual deviations of the mounting plate w.r.t. the center of the base using the rigid body model presented in Appendix B. Table 1 listed the averaged deviations obtained from all four sets of targeted dowel pin offsets. With an offset of 10 μm at EC-1 (Set 1), the deviation of the mounting plate w.r.t. the center of the base was less than 1 μm along the x- and y-axis, and 22 μrad about the z-axis. Even when all dowel pins were displaced (Set 4), the deviations along the x- and y-axis were less than 1.3 μm and 67 μrad about the z-axis. Hence, these experiments show that the elastic contacts are effective in averaging out the errors contributed by the dowel pin offsets.

In addition, the analytical results also agree well with the experimental results for all four sets. The results from Set 1 and Set 3 show that the equilibrium positions of the EC are well predicted by the model. As for Set 2, it is observed that the measured deviation about the z-axis is slightly lower than the predicted values because the measured equilibrium positions of EC-2 and EC-4 are lower than the desired positions. From Set 4, the measured deviations are higher than the predictions because the measured equilibrium positions of EC-1 and EC-2 are about 1 μ higher than the desired positions. As a result, Set 2 and 4 demonstrated the sensitivity of the experimental investigations whereby over or under displacing the dowel pins will affect the results. Nevertheless, all these investigations have shown that the presented model can be used to predict the 3-DOF planar motion deviations from the mounting plate when subjected to dowel pin offsets and other forms of manufacturing errors.

Another experiment was conducted to evaluate the repeatability of the mounting plate. A target block was mounted underneath the mounting plate (Fig. 10) and it provided two orthogonal flat surfaces, which were measured by another two capacitive probes

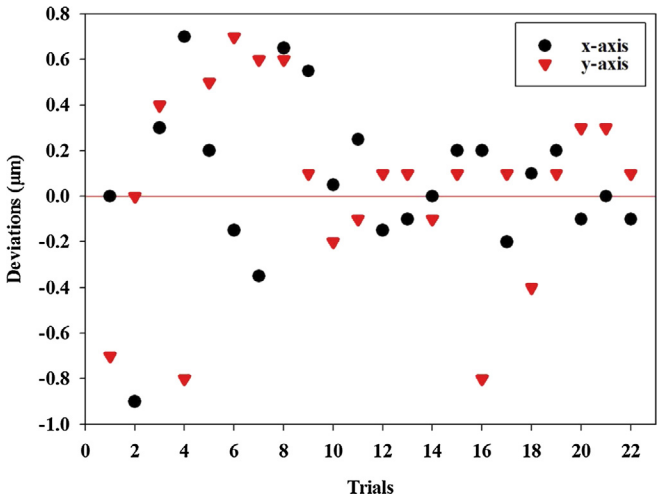

Fig. 14. Repeatability of the mounting plate w.r.t the center of the base recorded from taking it away and re-mounting it onto the base for more than 20 trials.

mounted in the base as shown in Fig. 12a. A base with four fixed dowel pins but without the flexure-based mechanisms was used to conduct the experiment. For more than 20 trials, the mounting plate was removed and re-assembled back to the base guided by the dowel pins. For each trial, the mounting plate was pushed flat to surface of the base and the capacitive probes recorded the deviations along the x- and y-axis. Fig. 14 plots the results, which show that the deviations were less than 1 μm obtained from those trails. In addition, the results also show that the friction between the dowel pin and flexure surfaces could have affected the deviations where the first 10 trials produced higher deviations as compared to the next 10 trails. With materials being removed and the surfaces being set in after the first 10 trials, less friction between the surfaces have caused the next 10 trails to produce lower deviations. Most importantly, these results show that the deviations were repeatable up to sub-micron levels during those trials.

5. Repeatability and error sensitivity

As the mounting plate is designed based on the principle of elastic averaging, by increasing the amount of elastic contacts on the mounting plate should improve the repeatability. In this work, the presented analytical model was also used to conduct further analyses on the repeatability of the mounting plate w.r.t. the number of elastic contacts.

5.1. Stiffness w.r.t. the number of elastic contacts

Numerical analyses using ANSYS16 were conducted to determine the stiffness of the mounting plate having different number of elastic contacts, i.e., from 4 to 20 with an increment of 2 elastic contacts, and also compared against the stiffness predicted by the presented model derived in Section 4.1. Predictions on the stiffness of each mounting plate were made from three separate analytical analyses. The first analysis used a complete analytical model, which is expressed in Eq. (18), where the main body has finite stiffness and the coupling effect between neighboring elastic contacts. In this analysis, λ was estimated at 5% in Eq. (15) for r_i = 65 mm (see Appendix C). The second analysis used an incomplete model where it accounted for the main body having finite stiffness but excluded the coupling effect, i.e., λ = 0. The third analysis used a model that only summed up the stiffness matrix of the elastic contacts whereby the main body was considered to have infinite stiffness and elas-

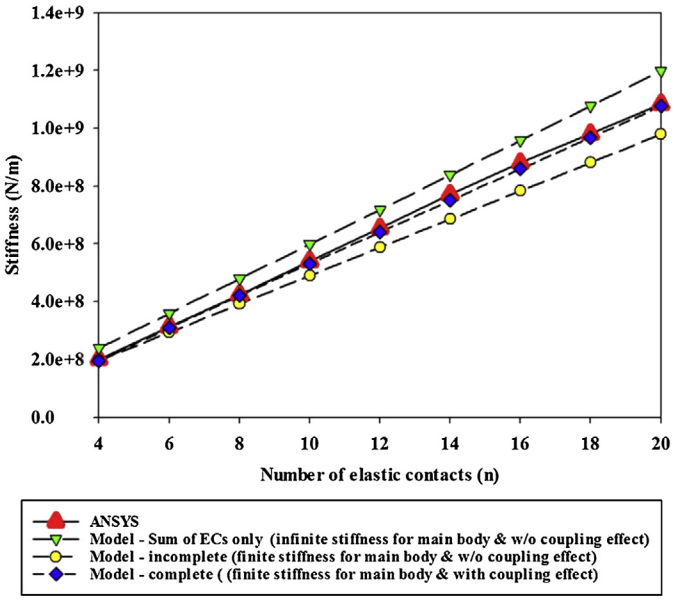

Fig. 15. Stiffness of the mounting plate w.r.t. the number of elastic contacts predicted by the numerical and analytical analyses.

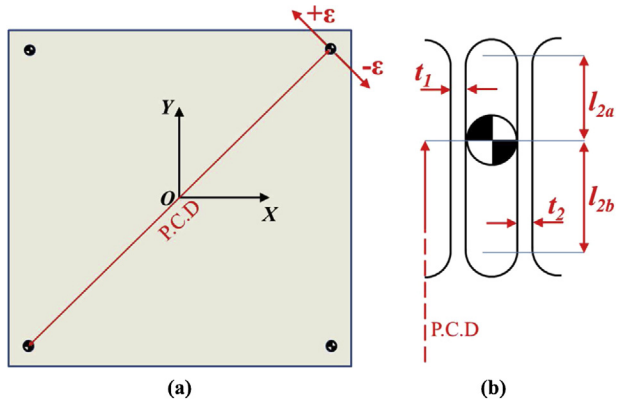

Fig. 16. Source of errors: (a) from the location of dowel pins and (b) from the elastic contacts.

tic contacts are not considered as one continuum body. Hence, it excluded $\mathbf{C}_i^B$ and the coupling effect from Eq. (18).

Fig. 15 plots the stiffness of the mounting plate w.r.t. the number of elastic contacts, n, predicted from the numerical and those three analytical analyses. It shows that the stiffness of the mounting plate increases linearly as n increases. It also shows that the stiffness predicted by the model, which only accounts for the stiffness of the elastic contacts, are higher compared to the numerical results. The stiffness predicted by the model, which accounts for the compliance of the main body but excludes the coupling effect, are lower than the numerical results while the predictions from the complete model agree with the numerical results. Refer to Table 2, the numerical analysis predicted the stiffness of the mounting plate with $n = 4$ (current prototype) to be 2.01×10^8 N/m while the complete model predicted 1.97×10^8 N/m. These numerical and analytical results can be considered accurate since the stiffness of the current prototype was indirectly evaluated from the experimental investigations conducted in Section 4.3. On the other hand, the model, which only account for the stiffness of the elastic contacts, predicted a stiffness value that is 19.4% higher as compared to the numerical result. Hence, it shows that the compliance of the body, $\mathbf{C}_i^B$, does contribute to the stiffness of the mounting plate with $n = 4$ (note: no coupling effect between neighboring elastic contacts for $n = 4$ since $\phi = 90^\circ$). However, it is also noticeable that such contribution drops as n increases. This shows that the overall compliance of the elastic contacts dominates the compliance of the mounting plate when n increases to certain amount. Hence, the model, which only account for the stiffness of the elastic contacts, still works well for $n > 10$ in this case.

By considering the stiffness of the main body while excluding the coupling effect, the incomplete model offers more consistent predictions on the stiffness where the average error is 8% and maximum error at 10.6%. With an average error of less than 3%, the complete model provides a good prediction on the overall stiffness of the mounting plate w.r.t. the number of elastic contacts. These results show that the compliance of the main body and the coupling effect have significant contributions to the stiffness of the mounting plate throughout the increment of n. Even without the estimated percentage for the coupling effect, the analytical predictions from the model that accounts the compliance of the main body agree well with the numerical results throughout the increment of n. Yet the inclusion of the coupling effect between the neighboring elastic contacts further improve the accuracy of the analytical model. Consequently, the complete model was used to conduct the analytical simulations to predict the error sensitivity of the mounting plate due to manufacturing errors and to determine how well the principle of elastic averaging can average out these errors.

5.2. Error sensitivity

The analytical simulations that predicted the error sensitivity of the mounting plate due to fabrication errors were conducted based on a group of n, i.e., 4, 8, 12, 16, 20, 25, 50, 100, 250, and 500. For each n, 100 iterations were conducted to determine the deviations along the x- and y-axis, and about the z-axis. At each iteration, random errors were injected into the critical parameters, e.g., the locations of the dowel pins and the thickness of the flexures. Subsequently, the standard deviations along the x- and y-axis, and about the z-axis from those 100 iterations were obtained and used to reflect the repeatability of the mounting plate among the 100 sets of random errors.

The critical parameters that were used in the simulations are illustrated in Fig. 16. The location of a dowel pin is defined by the Pitch Center Diameter (P.C.D.) and the offsets normal to the flexures. The P.C.D. will affect the location of dowel pin w.r.t. the center of the base, r_i, as illustrated in Fig. 5 and coupling it with the offsets normal to the flexure provide the position errors in the x–y plane. Within each elastic contact, the thickness and length of the flexure are the influential parameters, and the thickness between the pair of flexures can vary, i.e., $t_1 \neq t_2$. The P.C.D. will also affect the stiffness of the flexures as it changes the location of the dowel pin and affects the loading point since $l_{2a} \neq l_{2b}$. Hence, the three main critical parameters are the offsets of the dowel pins normal to the flexures, the P.C.D. of each pair of dowel pins and the thickness of the flexures.

The first set of simulations provided the repeatability of the mounting plate due to the random errors injected into the offset of dowel pin normal to the flexure and the P.C.D. of each pair of dowel pins. The maximum offset of the dowel pin was set at half of the maximum allowable yield stress of the material of the mounting plate and the potential positioning error of a CNC machine, i.e., 50 μm. Accounting for both conditions, the random offset was set within a range of ±0–20 μm for the offset of dowel pin normal to the flexure and ±0–90 μm for the P.C.D. Fig. 17 plots the standard deviations of the mounting plate along the x- and y-axis, and about the z-axis w.r.t. the increment of the number of elastic contacts due to random errors injected into the offset of dowel pin normal to the flexure and the P.C.D.

Table 2
Numerical and analytical predictions of the stiffness of the mounting plate w.r.t. the amount of elastic contacts.

n	Numerical results	Model – sum of ECs only (infinite stiffness for main body and no coupling effect)		Model – incomplete (finite stiffness for main body and no coupling effect)		Model – complete (finite stiffness for main body and coupling effect)	
	Stiffness 1×10^8 (N/m)	Stiffness 1×10^8 (N/m)	Error (%)	Stiffness 1×10^8 (N/m)	Error (%)	Stiffness 1×10^8 (N/m)	Error (%)
4	2.01	2.40	19.40	1.97	1.91	1.97	1.91
6	3.13	3.59	14.85	2.95	5.65	3.07	1.83
8	4.24	4.79	12.96	3.94	7.19	4.16	1.90
10	5.40	5.99	10.90	4.92	8.89	5.25	2.89
12	6.55	7.19	9.74	5.91	9.84	6.32	3.49
14	7.71	8.39	8.83	6.89	10.59	7.39	4.05
16	8.81	9.59	8.84	7.87	10.58	8.47	3.88
18	9.82	1.08	9.82	8.86	9.78	9.53	2.90
20	10.8	12.0	10.50	9.84	9.22	10.6	2.21

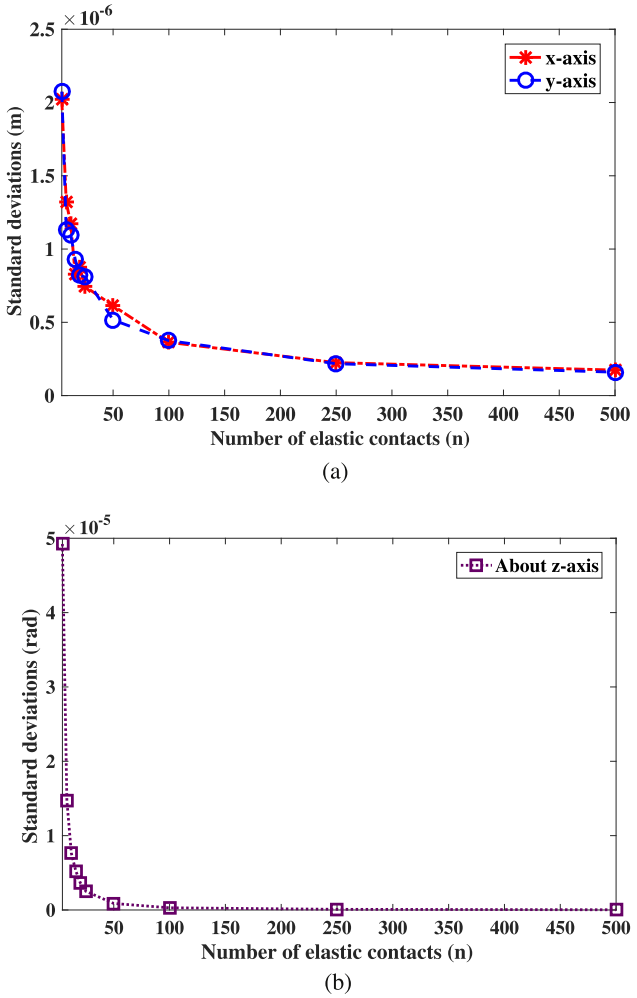

Fig. 17. Standard deviations of the mounting plate (a) along the x- and y-axis, and (b) about the z-axis w.r.t. the number of elastic contacts due to the random errors injected into the offset of dowel pin normal to the flexure and the P.C.D of each pair of dowel pins.

Fig. 17a shows that the mounting plate with $n = 4$ produced a repeatability of ~2.1 μm along the x- and y-axis from the analytical simulations. As n increased, the repeatability of the mounting plate increased, which can be seen from the decrease of the standard deviations. With $n = 20$, the standard deviations along the x- and y-axis fell below 1 μm and continue to decline and stabilize after $n > 250$. Similar trend is observed for the angular deviation about the z-axis (Fig. 17b) except there was also no deviation after $n > 100$. The results also suggest that the principle of elastic averaging is effective in averaging out the random errors injected into the offset of dowel pin normal to the flexure and the P.C.D.

The second set of simulations provided the repeatability of the mounting plate due to the random errors injected into the thickness of the flexures. These simulations were conducted to determine the effectiveness of elastic averaging towards improving the repeatability of a mounting plate that could be rapid fabricated by an additive manufacturing process. Assuming that the fabrication is done either by the Selective-Laser-Sintering (SLS) or Electron-Beam-Melting (EBM), the maximum dimensional tolerances are assumed to be ~150–200 μm. Hence, the random offset for each flexure thickness was set within a range of ±0–200 μm.

Fig. 18 plots the standard deviations of the mounting plate along the x- and y-axis, and about the z-axis w.r.t. the increment of the number of elastic contacts due to the random thickness of each flexure within the elastic contacts. From Fig. 18a, the simulation results show that the random thickness errors can be averaged out effectively even at $n = 4$, which produced a repeatability of ~0.165 μm and ~0.15 μm along the x- and y-axis respectively. With $n = 8$, the standard deviations fell below 0.1 μm for both x- and y-axis, and less than 0.45 μrad about the z-axis as shown in Fig. 18b. Hence, this set of simulated results suggest that the principle of elastic averaging allows the rapid fabricated parts to be precisely located even if the elastic features cannot be accurately fabricated.

Lastly, a third set of simulations was conducted to determine the repeatability of the mounting plate due to the random errors injected into all critical parameters. From the simulated results plotted in Fig. 19, it is observed that the standard deviations when $n = 4$ are close to those plotted in Fig. 17. In addition, the rate of change of the deviations w.r.t. n is similar between these two sets of simulations. These comparisons suggest that the actual locations of the dowel pins have huge influence in how well the mounting plate can be precisely located w.r.t. the base. This observation is back by the simulated results plotted in Fig. 18, which suggest that varying flexure thickness has less influence in the deviations using elastic averaging. Nevertheless, all the simulated results have shown that by increasing n will reduce the deviations. Most importantly, all these results highlighted that rapid fabricated parts from casting, 3D printing, waterjet, laser cutting etc., can be precisely located, and the principle of elastic averaging is the solution to make these parts useable in precision engineering.

6. Quick estimation of the standard deviations w.r.t. the number of elastic contacts using $1/\sqrt{n}$

The accuracy of a part with elastic averaging features is stated to be on the order of $\sqrt{n}$ times better than its rigid counterpart [20] and its repeatability is approximately inversely proportional to $\sqrt{n}$

Table 3
Analytical predictions and estimation of the deviations of the mounting plate along the x- and y-axis, and about the z-axis due to the random errors injected into all critical parameters w.r.t. the number of elastic contacts.

n	Analytical predictions			$\rho/\sqrt{n}$		$(n^*\rho)/(n\sqrt{n})$	Error (%)		
	ΔX (m)	ΔY (m)	ΘZ (rad)	ΔX (m)	ΔY (m)	ΘZ (m)	ΔX	ΔY	ΘZ
$4 = n^*$	2.22×10^{-6}	2.11×10^{-6}	4.80×10^{-5}	–	–	–	–	–	–
8	1.36×10^{-6}	1.50×10^{-6}	1.83×10^{-5}	1.57×10^{-6}	1.49×10^{-6}	1.70×10^{-5}	15	1	7
12	1.13×10^{-6}	1.08×10^{-6}	8.61×10^{-6}	1.28×10^{-6}	1.22×10^{-6}	9.23×10^{-6}	13	12	7
16	9.61×10^{-7}	9.77×10^{-7}	4.92×10^{-6}	1.11×10^{-6}	1.05×10^{-6}	6.00×10^{-6}	15	8	22
20	9.82×10^{-7}	1.01×10^{-6}	4.18×10^{-6}	9.91×10^{-7}	9.43×10^{-7}	4.29×10^{-6}	1	7	3
25	7.50×10^{-7}	8.31×10^{-7}	2.75×10^{-6}	8.86×10^{-7}	8.43×10^{-7}	3.07×10^{-6}	18	2	12
50	5.36×10^{-7}	6.04×10^{-7}	9.60×10^{-7}	6.26×10^{-7}	5.96×10^{-7}	1.09×10^{-6}	17	1	13
100	3.78×10^{-7}	3.63×10^{-7}	3.20×10^{-7}	4.43×10^{-7}	4.22×10^{-7}	3.84×10^{-7}	17	16	20
250	2.52×10^{-7}	2.79×10^{-7}	1.12×10^{-7}	2.80×10^{-7}	2.67×10^{-7}	9.71×10^{-8}	11	4	13
500	1.66×10^{-7}	2.03×10^{-7}	6.19×10^{-8}	1.98×10^{-7}	1.89×10^{-7}	3.48×10^{-8}	19	7	45

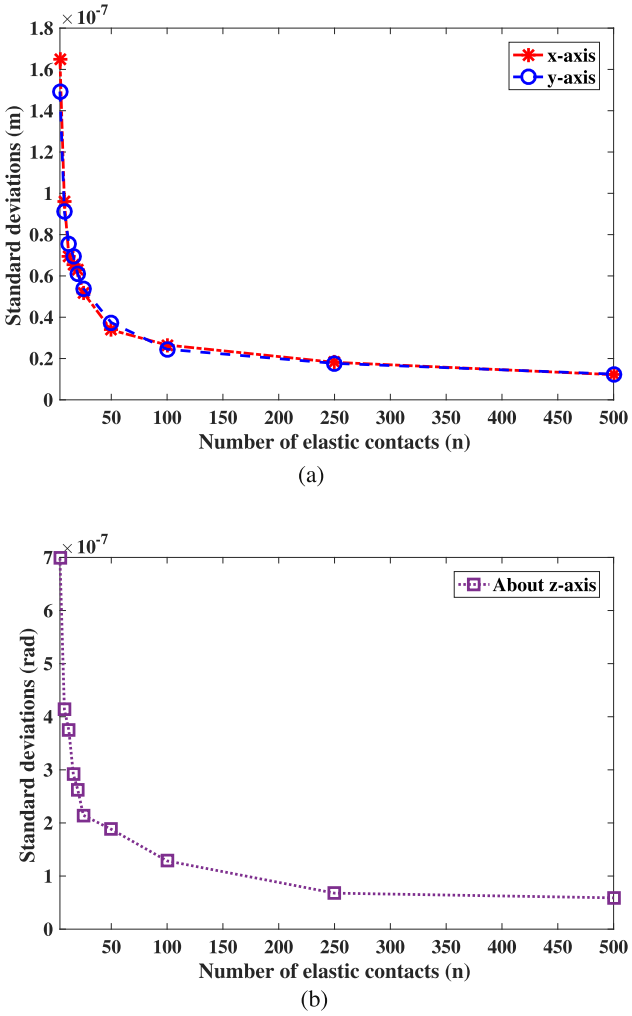

Fig. 18. Standard deviations of the mounting plate (a) along the x- and y-axis, and (b) about the z-axis w.r.t. the number of elastic contacts due to the random errors injected into the flexure beam thickness.

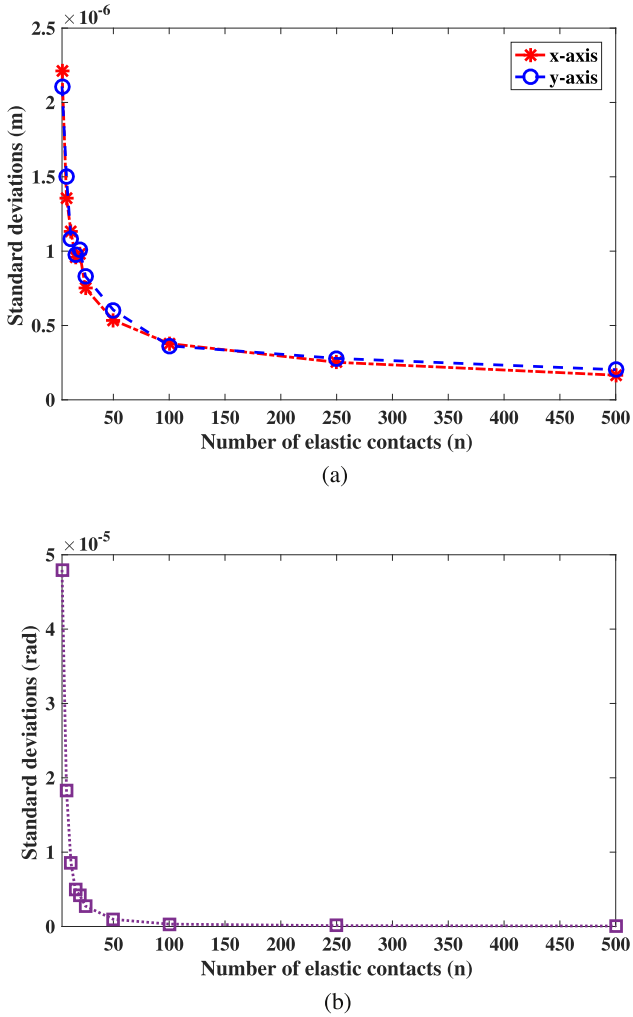

Fig. 19. Standard deviations of the mounting plate (a) along the x- and y-axis, and (b) about the z-axis w.r.t. the number of elastic contacts due to the random errors injected into all critical parameters.

[5]. Recent literatures [6,7] have also "loosely" demonstrated the repeatability of elastic averaging is $1/\sqrt{n}$. In this work, the analytical simulations that are presented in Section 5.2 were also used to determine whether the standard deviations will decrease based on a trend of $1/\sqrt{n}$ as n increases. Using the last set of analytical simulation results presented in Section 5.2 as example, Fig. 20 and Table 3 show that the standard deviations of the mounting plate along the x- and y-axis due to the random errors injected into all critical parameters do decrease linearly w.r.t. n.

To verify whether this decreasing trend follows $1/\sqrt{n}$, it is important to first determine the value of the reference deviation, ρ, which is given as

$$\rho = \sqrt{n^*}\Delta(n^*) \tag{25}$$

where $\Delta(n^*)$ represents the deviations ΔX, ΔY or ΘZ of a mounting plate with (n^*) number of elastic contacts. Subsequently, the

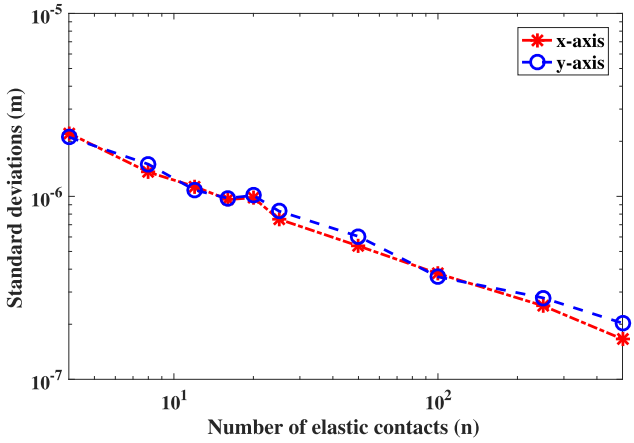

Fig. 20. Log-Log plot of the standard deviations of the mounting plate along the *x*- and *y*-axis w.r.t. the number of elastic contacts due to the random errors injected into all critical parameters.

deviations along the *x*- and *y*-axis w.r.t. other *n* can be estimated from

$$\Delta(n) = \frac{\rho}{\sqrt{n}} \tag{26}$$

The deviation about the *z*-axis w.r.t. other *n* is given as

$$\Theta Z(n) = \frac{n^* \rho}{n\sqrt{n}} \tag{27}$$

Eqs. (25)–(27) were used to estimate the deviations of the mounting plate along the *x*- and *y*-axis, and about the *z*-axis w.r.t. the increment of *n*, and the estimated results are listed in Table 3. In this case, the first set of analytical deviations obtained from a mounting plate with $n^* = 4$ were used to determine the reference deviations using Eq. (25). Here, the reference deviations, i.e., ΔX, ΔY and ΘZ, are determined as 4.43 μm, 4.22 μm, and 95.9 μrad respectively. Subsequently, Eqs. (26) and (27) were used to estimate the deviations of the mounting w.r.t. the increment of *n* listed in Table 3. The errors between the analytical predictions and the estimated deviations are listed on the right of Table 3. The comparisons show that the deviations do decrease at the trend of $1/\sqrt{n}$. Except for the ΘZ with $n = 500$, the results show that using $1/\sqrt{n}$ can provide a quick and reasonable estimation of the deviations without running those intensive simulations as presented in Section 5.2. Hence, this work shows that a designer can first model a mounting plate with 4 elastic contacts to predict the deviations and subsequently use $1/\sqrt{n}$ to estimate the deviations of the mounting plate w.r.t. different *n*.

In summary, the first-order analytical model, which can be derived from the proposed general modeling approach, should be used to predict the 3-DOF in-plane deviations first. Next, quick but less accurate estimations of the deviations w.r.t. other elastic contacts can be obtained using $1/\sqrt{n}$ to determine the desired number of elastic contacts. Subsequently, the first-order analytical model should be used to obtain more accurate predictions of the deviations of the mounting plate with the selected number of elastic contacts. The analytical model is necessary because finite element analysis using numerical simulation platforms such as ANSYS16 etc., does not provide angular displacement prediction. Finite element analysis should be conducted on the final design to ensure that the second-order effects are accounted for. This is because the first-order analytical model does not account for such second-order effects (see Appendix C). By following these design steps and using the presented analytical models, a designer can design, and develop assembly parts with elastic features for precise alignment and assembly.

Table 4
Design parameters for the developed prototype.

Parameter	
Radius, *r* (mm)	65
Length of flexure, *l* (mm)	12
Thickness of flexure (mm)	1.5
Width of flexure (mm)	3
Dowel pin diameter (mm)	3
Slot gap (mm)	2.95
Equivalent length of each segment, *d* (mm)	55
Equivalent area of each segment (mm^2)	5.14
Segment width (mm)	3

7. Conclusion

This paper has presented the concept designing parts with elastic averaging features that can "average out" the uncertainty in dimension tolerances and manufacturing errors as a collective system at very low cost. The key concept was the use of N_s^2 pairs of "rigid" pins and defined "elastic" flexure elements to form a pair of interfacing parts that can achieve precise assembly. A generic modeling approach is presented to establish a first-order analytical model that predicts the alignment errors and the repeatability of these interfacing parts. Experimental investigations show that a fabricated part with four simple elastic averaging features was capable of achieving less than 1.3 μm and 66.1 μrad of alignment errors with another mating part even after 30 μm errors were being purposefully introduced to the mating features. Experimental investigations also show that the repeatability of the fabricated part remained at sub-micron level after more than 20 trials of removing and assembling. Lastly, analytical simulations show that the repeatability of the part can improve significantly by increasing the number of these features. Most importantly, the error sensitivity of these parts is low for varying the thickness of these features. In summary, these investigations demonstrated that rapid fabricated parts from casing, abrasive waterjet machining, laser cutting, and AM etc., can be designed with such elastic features to mate with other parts having reciprocal rigid pins to achieve precise alignment and assembly. As a result, the assemblies of parts made by these rapid fabrication processes can be as precise as those made from conventional milling, turning, and grinding processes.

Appendix A. Parameters

The $120 \times 120\ mm^2$ mounting plate prototype is made of aluminum 7075-T6 with Young's Modulus of 71GPa and the remaining parameters are listed in Table 4. For the developed prototype, the slot gap is 50 μm smaller than the diameter of the dowel pin. Hence, the contact surface, 2*W*, will be 5% of the total flexure length for Eq. (13).

For the numerical and analytical simulations presented in Section 5, the dimension of the mounting plate was increased to $150 \times 150\ mm^2$ to accommodate more than four elastic contacts. The equivalent length and thickness of each segment of the main body are approximated from $r - (l/2)$, and $2\pi(r+l)/4$. As a result, the equivalent length and area of the main body are 59 mm, and $6.93\ mm^2$ respectively. Since the ANSYS CAD model cannot simulate press-fitting of dowel pin between the pair of flexures, the slot gap is kept similar to the diameter of the dowel pin, i.e., 3 mm. Hence, the contact surface, 2*W*, is zero for both the numerical and analytical simulations while the remaining parameters are similar to those listed in Table 4.

Table 5
Numerical and analytical predictions of the stiffness of the mounting plate with 4 elastic contacts w.r.t. different P.C.D configurations.

P.C.D. (mm)	Numerical results	Model – sum of ECs (infinite stiffness for main body)		Model – $\lambda = 0$ (finite stiffness for main body)	
	Stiffness 1×10^8 (N/m)	Stiffness 1×10^8 (N/m)	Error (%)	Stiffness 1×10^8 (N/m)	Error (%)
210	1.86	2.40	28.56	1.93	3.68
190	1.88	2.40	27.19	1.94	2.91
170	1.91	2.40	25.33	1.95	1.81
150	1.95	2.40	22.99	1.96	0.42
130	2.01	2.40	19.40	1.97	1.91
110	2.04	2.40	17.30	1.98	2.84
90	2.11	2.40	13.66	2.01	4.80
70	2.21	2.40	8.43	2.04	7.70
50	2.59	2.40	7.55	2.09	19.29
40	2.62	2.40	8.42	2.13	18.53

Table 6
Numerical and analytical predictions of the stiffness of a mounting plate with 6 elastic contacts w.r.t. different P.C.D configurations.

P.C.D. (mm)	Numerical results (N/m)	λ (%)	Analytical results (N/m)	Error (%)
210	2.92×10^8	0.55	2.91×10^8	0.30
190	2.93×10^8	0.96	2.93×10^8	0.07
170	2.99×10^8	1.66	2.96×10^8	0.87
150	3.04×10^8	2.88	3.00×10^8	1.32
130	3.13×10^8	4.99	3.07×10^8	1.83
110	3.22×10^8	8.64	3.19×10^8	0.93
90	3.35×10^8	14.97	3.38×10^8	0.86
70	3.54×10^8	25.93	3.71×10^8	4.79
50	4.35×10^8	44.92	4.30×10^8	1.18
40	5.15×10^8	77.80	5.23×10^8	1.44

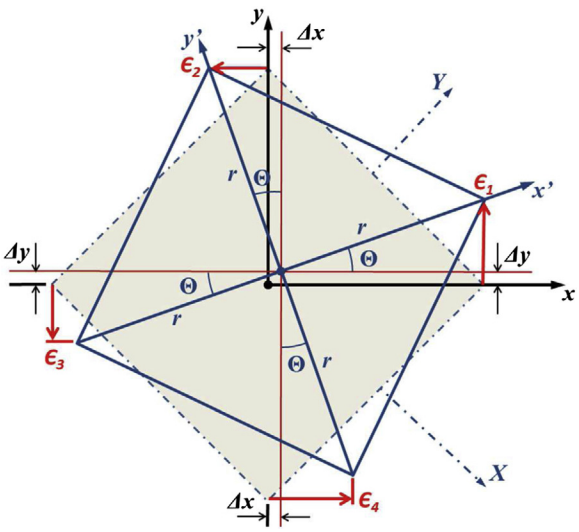

Fig. 21. Rigid body motion of the mounting plate due to the in-plane equilibrium displacements.

Appendix B. Rigid body model

The measured in-plane displacements from the elastic contacts of the mounting plate prototype (Fig. 10) are the actual equilibrium positions (listed in Table 1) that were used to determine the actual deviations of the mounting plate w.r.t. the center of the base. Fig. 21 illustrates an exaggerated rigid body motion of the mounting plate caused by these in-plane equilibrium displacements. The mounting plate is rotated anti-clockwise by 45° about the global coordinate frame, $O\{X, Y\}$, and a new frame, $o\{x, y\}$, is attached to it. Assuming that all elastic contacts are rigidly connected by the main body with radius, r, and small magnitude for all in-plane displacements, the relationships between the actual equilibrium positions and the deviations along the x- and y-axis w.r.t. the frame o are given as follows

$$\begin{aligned} \epsilon_1 &= r\Theta + \Delta y \\ r\Theta &= \epsilon_2 + \Delta x \\ r\Theta &= \epsilon_3 + \Delta y \\ \epsilon_4 &= r\Theta + \Delta x \end{aligned} \tag{28}$$

Based on Eq. (28), the deviations along the x- and y-axis w.r.t. the frame o is expressed as

$$\begin{aligned} \Delta x &= (\epsilon_4 - \epsilon_2)/2 \\ \Delta y &= (\epsilon_1 - \epsilon_3)/2 \end{aligned} \tag{29}$$

Based on Eq. (29), the deviations along the x- and y-axis, and about the z-axis w.r.t. the origin frame O is expressed as

$$\begin{aligned} \Delta X &= \Delta x \cos 45 + \Delta y \cos 135 \\ \Delta Y &= \Delta x \sin 45 + \Delta y \sin 135 \\ \Theta Z &= (\epsilon_1 - \Delta y)/r \end{aligned} \tag{30}$$

Appendix C. Estimation of coupling effects

As mentioned in Section 3.2, the coupling effect is not present for spacing ≥90°. To demonstrate that λ in Eq. (15) is equal zero for a mounting plate with 4 elastic contacts, two separate analyses were conducted. The first analysis used an analytical model that only summed up the stiffness matrix of the elastic contacts whereby the main body was considered to have infinite stiffness and elastic contacts are not considered as one continuum body. Thus, the model excluded $\mathbf{C}_i^B$ and the coupling effect from Eq. (18). The second analysis used the proposed first-order analytical model, which accounts for the finite stiffness of the main body and the coupling effect. For a mounting plate with $n = 4$, λ in Eq. (15) was set to zero. By changing the P.C.D. from 40 to 210 mm with an increment of 10 mm, the stiffness of a mounting plate with 4 elastic contacts

was predicted via the numerical simulations (ANSYS16) and the two analytical models. 40 mm was chosen to be the shortest possible P.C.D. configuration because two neighboring elastic contacts cannot be formed from a dimension smaller than this value.

Based on the obtained numerical and analytical results listed in Table 5, it is clear that the analytical model that only summed up the stiffness of the elastic contacts could not predict the change of stiffness w.r.t. the different P.C.D. configurations. On the other hand, the proposed first-order analytical model was able to provide a good prediction of the stiffness even as the P.C.D. configuration changed. However at P.C.D. between 40 and 50 mm, the analytical model was unable to provide accurate prediction of the stiffness. Although having a P.C.D. configuration that is lesser than 50 mm may not be practical or useful in practice, this analysis still highlighted that the first-order analytical model does not account for the second-order effects that were exhibited from the mounting plates with very short P.C.D. configurations. These numerical predictions suggest that the coupling effect does affect the stiffness characteristic of the mounting plate with 4 elastic contacts when all these elastic contacts are very close to each other. Hence, it is always necessary to conduct a finite element analysis for the final design to ensure that such second-order effects are accounted for. Nevertheless, this analysis has shown that the first-order analytical model is capable of providing a good prediction of the stiffness w.r.t. the different P.C.D. configurations for most general cases. Most importantly, it also demonstrated that the λ in Eq. (15) can be assumed as zero for a mounting plate with 4 elastic contacts for most of the practical P.C.D. configurations.

Refer to Eq. (9), it is clear that the stiffness matrix of a beam element in 3-DOF planar motion does not account for the non-diagonal components that contribute to the coupling effect. As a result, an indirect approach was used to estimate the value of λ for a mounting plate with more than 4 elastic contacts. Using Eq. (14) and the flexure parameters given in Appendix A, the stiffness matrix of each elastic contact w.r.t. the global frame (from a mounting plate with 4 elastic contacts) is

$$\mathbf{K}_i^T = \begin{bmatrix} 5.99\times10^7 & 4.66\times10^7 & 6.12\times10^5 \\ 4.66\times10^7 & 5.99\times10^7 & -6.12\times10^5 \\ 6.12\times10^5 & -6.12\times10^5 & 5.69\times10^4 \end{bmatrix} \quad (31)$$

This stiffness matrix of an elastic contact, which is oriented at 45°, was used because it provides the highest percentage of coupling effect compared to other angle orientation. From Eq. (31), it shows that the non-diagonal components, i.e., k_{12} or k_{21}, is 77.8% of the diagonal components, i.e., k_{11} or k_{22}. Hence, it also suggests that the maximum coupling effect between two nearest elastic contacts will be 77.8%. However, this coupling effect is governed by the locations of both elastic contacts, i.e., the angle, ϕ, between them and their distance, r, w.r.t. the center of the mounting plate. As shown in Fig. 16, r is half of the P.C.D. While $\cos\phi$ is used to represent the space between each elastic contact in Eq. (15), the percentage of coupling effect, λ, also changes according to the P.C.D. configuration.

The diagonal component, k_{11}, of a stiffness matrix of a mounting plate with 6 elastic contacts w.r.t. the P.C.D. was predicted via the numerical simulations (ANSYS16) and the analytical model presented in Section 3. By changing the P.C.D. from 40 to 210 mm with an increment of 10 mm, the values of k_{11} obtained from both the numerical and analytical results are listed in Table 6. With 77.8% selected as λ for P.C.D. of 40 mm, the respective λ for each incremental value of P.C.D. was estimated by a division of $\sqrt{3}$ of previous λ, e.g., the λ for P.C.D. of 50 mm will be $77.86/\sqrt{3}$. This approach provided a good estimation of the λ for each P.C.D. Using these λ, the predictions obtained from the analytical model agree well with the numerical simulation results. As a result, $\lambda = 5\%$ was used for mounting plate with $r = 65$ mm in Section 5.1.

Appendix D. Numerical simulation parameters

In this work, the numerical simulations were all conducted using ANSYS16 WORKBENCH under the static structural analysis. For all the analyses, the mesh property was selected as "Hex Dominant" and the mesh type was selected as "All Quad". The sizing of the mesh was selected as "Medium" for the first meshing process. Next, all the flexure beams were selected for secondary fine meshing process. The Young's Modulus and the Poisson's Ratio the mounting plate were selected to be 71 GPa, and 0.33 respectively. Structure steel was selected as the material for each dowel pin, which by default gives a Young's Modulus of 200 GPa and Poisson's Ratio of 0.3.

Appendix E. Supplementary data

Supplementary data associated with this article can be found, in the online version, at http://dx.doi.org/10.1016/j.precisioneng.2017.02.003.

References

[1] Evans C. Precision Engineering: An Evolutionary View. Cranfield, UK: Cranfield Press; 1989.
[2] Jones RV. Instruments and Experiences. New York, USA: John Wiley; 1988.
[3] Plummer W. Precision: How to achieve a little more of it, even after assembly. In: Fifth International Symposium on Robotics and Manufacturing; 1994.
[4] Yoder P, Vukobratovich D. Optical Mechanical Systems Design. 4th ed. CRC Press; 2015.
[5] Slocum A. Precision Machine Design. Dearborn, MI, USA: SME; 1995.
[6] Slocum A, Weber A. Precision passive mechanical alignment of wafers. IEEE JMEMS 2003;12(Dec (6)):826–34.
[7] Willoughby P. Elastically Averaged Precision Alignment (Ph.D. thesis). Cambridge, MA: Massachusetts Institute of Technology; 2005, June.
[8] Tolerance rings, USA Tolerance Rings, webpage source 2017, http://www.usatolerancerings.com/.
[9] Rowe K, Dickrell DJ, Sawyer WG. Interrupted measurement repositioning using elastic averaging. Tribol. Lett 2015;59.
[10] Jiang L, Pandraud G, French PJ, Spearing SM, Kraft M. A novel method for nanoprecision alignment in wafer bonding applications. J. Micromech. Microeng 2007;17.
[11] Gurung S. Passive Alignment of Micro-Fluidic Chips Using the Principle of Elastic Averaging (Master thesis). Louisiana State University; 2007.
[12] Slocum A. Design of three-groove kinematic couplings. Precis. Eng 1992;14(April (2)):67–76.
[13] Bathe KJ. Finite Element Procedures in Engineering Analysis. Englewood Cliffs, NJ: Prentice-Hall; 1982.
[14] Strang G. Introduction to Applied Mathematics. Cambridge, MA: Wellesley-Cambridge Press; 1986.
[15] Rao SS. Mechanical Vibrations. 3rd ed. New York: Addison-Wesley Publishing Company; 1995.
[16] Timoshenko S, Goodier JN. Theory of Elasticity. York, PA: McGraw-Hill Inc.; 1951.
[17] Barber JR. Elasticity. 2nd ed. Netherlands: Springer; 2004.
[18] Slocum A. Fundamental principles. In: Fundamental of Design. MA: Cambridge-MIT Institute; 2007 http://web.mit.edu/2.75/fundamentals/FUNdaMENTALS.html.
[19] Teo TJ, Yang G, Chen I-M. Compliant manipulators. In: Handbook of Manufacturing Engineering and Technology. London: Springer; 2014. p. 2229–300.
[20] Jones RV. Some uses of elasticity in instrument design. J. Sci. Instrum 1962;39(May):193–203.